Geometric algorithm for efficient coincident detection of gravitational waves

C. A. K. Robinson,[1,*] B. S. Sathyaprakash,[1,+] and Anand S. Sengupta[1,2,‡]

[1]*School of Physics and Astronomy, Cardiff University, 5, The Parade, Cardiff, United Kingdom, CF24 3AA*
[2]*LIGO Laboratory, California Institute of Technology, Pasadena, California 91125, USA*

(Received 7 May 2008; published 3 September 2008)

Data from a network of gravitational-wave detectors can be analyzed in coincidence to increase detection confidence and reduce nonstationarity of the background. We propose and explore a geometric algorithm to combine the data from a network of detectors. The algorithm makes optimal use of the variances and covariances that exist among the different parameters of a signal in a coincident detection of events. The new algorithm essentially associates with each trigger ellipsoidal regions in parameter space defined by the covariance matrix. Triggers from different detectors are deemed to be in coincidence if their ellipsoids have a nonzero overlap. Compared to an algorithm that uses uncorrelated windows separately for each of the signal parameters, the new algorithm greatly reduces the background rate thereby increasing detection efficiency at a given false alarm rate.

DOI: 10.1103/PhysRevD.78.062002 PACS numbers: 04.30.−w, 04.80.Nn, 95.55.Ym, 95.75.Pq

I. INTRODUCTION

Long baseline interferometric gravitational-wave (GW) detectors, such as the Laser Interferometer Gravitational-Wave Observatory (LIGO) [1], Virgo [2], and GEO 600 [3], are currently acquiring the best data ever. The data sets from the different detectors can be either brought together and analyzed phase coherently [4–7], or analyzed separately followed up by a coincidence analysis [6,8–15] of the triggers obtained. Coherent analysis maximizes signal visibility (i.e., gives the best possible signal-to-noise ratio in the likelihood sense) while the goal of coincidence analysis is to reduce and mitigate the nonstationary and non-Gaussian background noise. A recent comparison of coherent analysis *vis-à-vis* coincidence analysis under the assumption that the background noise is Gaussian and stationary has concluded that coherent analysis, as one might expect, is far better than coincidence analysis [16]. However, there are two reasons why current data-analysis pipelines prefer the latter over the former. First, since the detector noise is neither Gaussian nor stationary, coincidence analysis can potentially reduce the background rate far greater than one might think otherwise. Second, coherent analysis is computationally far more expensive than coincidence analysis and it is presently not practicable to employ coherent analysis.

A. The problem of coincident detection

In coincidence analysis (see, for example, Refs. [11–14,17–20]), data sets from each detector will be analyzed separately and the triggers from the end of the pipeline from different detectors compared with one another to identify triggers that might be in coincidence with one another. More precisely, the goal is to find if the parameters of a trigger (e.g., in the case of a coalescing binary the time of merger, the component masses and spins) from one detector are identical to those from another. Since the presence of noise causes errors in the measurement of parameters of an inherent signal, it is highly improbable that the same gravitational wave in different detectors can be associated with exactly the same set of parameters. However, it should be possible to detect signals in coincidence by demanding that the measured parameters lie in a sufficiently small range of each other [11–14,17,18]. Thus, we can revise the coincidence criteria as follows: triggers from different detectors are said to be in coincidence if their parameters all lie within a certain acceptable range. Events that pass the coincidence test are subject to further scrutiny but we shall focus in this paper on the coincidence test itself.

From the above discussion it is clear that an important aspect of coincidence analysis is the determination of the range of parameter values to be associated with each trigger. To this end, until recently, the LIGO Scientific Collaboration (LSC) has deployed a phenomenological method for assigning the ranges [11–14,17,18]. More precisely, one performs a large number of simulations in which a signal with a known set of parameters is added in software to the data which is then passed through the analysis pipeline. The pipeline identifies the most probable parameters with each injected signal and the ensemble of injected and measured parameters gives the distribution of the errors incurred in the measurement process. Given the distribution of the errors, one can choose a range for each parameter such that more than, say, 95% of the injected signals are detected in coincidence. Choosing wider windows will enable greater detection probability but also increases the rate of accidental triggers. On the contrary,

*C.Robinson@astro.cf.ac.uk
+B.Sathyaprakash@astro.cf.ac.uk
‡sengupta@ligo.caltech.edu

smaller windows decrease the false alarm rate but also reduce the detection probability. Recently, a Bayesian coincidence test has been proposed [21] as an alternative wherein one computes the likelihood of a candidate event as belonging to a distribution obeyed by true signals rather than the noise background. Unfortunately, measuring the distribution function when the parameter space is large could be computationally formidable [21] except when the parameters are independent.

B. A geometric approach to choosing coincident windows

In this paper we propose a new algorithm based on the metric (equivalently, the information matrix) defined on the signal manifold. The idea is very simple, even obvious, but leads to a great reduction in the background trigger rate. The advantages of the new algorithm are better appreciated by listing certain drawbacks of the phenomenological method. The drawbacks are quite naturally remedied in the new approach.

First, because the current method uses rectangular windows it ignores the correlations between different parameters. For instance, in the case of a chirping signal from a black hole binary the shape of the signal depends, among others, on the component masses. However, not all combinations of the two masses lead to signals that are easily distinguishable from one another. Indeed, at the lowest post-Newtonian (PN) order the waveform depends only on a certain combination of the masses called the *chirp mass*; binaries of different values for the two masses but the same chirp mass produce essentially the same signal. This degeneracy is broken when post-Newtonian corrections are included. Nevertheless, the two mass parameters continue to be highly correlated.

The second drawback is that the method employs windows of the same size throughout the parameter space while we know that errors in the measurement of the parameters depend, in some cases quite sensitively, on the parameters. Drawing again from our example of a binary, the error in the estimation of the chirp mass can vary by more than 2 orders of magnitude across the parameter space of interest in the case of systems that LIGO is expected to observe (see, e.g., [22–32]). Clearly, it is not optimal to deploy windows of the same size all over the parameter space.

Third, by not taking into account parameter covariances, the method entails independent tuning of several parameters at the same time. This could be a horrendous problem when dealing with signals characterized by many parameters. For instance, continuous radiation from a pulsar is characterized by the location of the pulsar, its spin frequency, the derivative of the frequency, and so on. These physical parameters are all not independent; the existence of covariances among them implies that the effect of variation in one parameter can be absorbed by another—thereby complicating the pipeline tuning procedure. In the case where parameters have perfect or near perfect covariances, variations of the parameters may not even lead to distinct signals at all. This further implies that it may not be necessary to tune each parameter separately, rather it should be enough to tune only a subset of the parameters or, more precisely, only the principal components. Furthermore, the method does not provide a unique set of windows, rather several possibilities could be worked out.

Finally, by using windows of the same size irrespective of the signal-to-noise ratio (SNR) of the trigger, the method suffers from an undesirably high false alarm rate, particularly in the tail of the SNR distribution. Needless to say, a successful detection of gravitational waves necessitates as clean a distribution of the SNRs as possible, with little contamination of the tails. One way of reducing the false alarm rate is by using tighter windows at higher SNRs. This is well motivated since true high-SNR events will be associated with smaller errors.

The geometric algorithm proposed in this paper quite naturally overcomes the drawbacks of the phenomenological method. The algorithm takes into account the correlations among the various parameters and deploys parameter- and SNR-dependent ellipsoidal windows defined by the Fisher information matrix using a single parameter. The most important consequence of the new algorithm is a great reduction in the background rate.

C. Organization of the paper

In Secs. II, III, and IV, we present and discuss the new algorithm to identify events in coincidence. The algorithm is comprised of two steps. The first step consists of associating each trigger with a p-dimensional ellipsoid. In the second step one tests if the ellipsoid associated with a trigger from one detector overlaps, or at least touches, an ellipsoid associated with a trigger from another detector. In Sec. V we apply the algorithm developed in Sec. II to the case of a transient chirp signal from a binary black hole. This will help us assess the extent to which the algorithm is helpful in reducing the background. Section VI concludes by summarizing the application of the new algorithm in real data-analysis pipelines and future prospects.

II. A GEOMETRIC COINCIDENCE ALGORITHM

This section begins with a brief introduction to the geometric formulation of signal manifold and metric introducing the terminology needed in later sections [33]. The metric so defined helps us in identifying ellipsoidal regions with a given point on the manifold whose size is chosen depending on the SNR and the parameter space region where the point lies. As an exercise to estimate the efficacy of the new coincidence algorithm we then compare the volume of the ellipsoid with that of a proper rectangular box enclosing the ellipsoid and aligned along the coordinate lines.

A. Scalar product, signal manifold, and metric

The problem of gravitational-wave data analysis was addressed in a geometric framework with the intention of understanding parameter estimation [29,30] and computational requirements for matched filtering [34–36]. In this framework, one thinks of the outputs of an ensemble of detectors as either finite- or infinite-dimensional vectors depending on whether one considers data streams as a discrete sampled set or the continuum limit of the same, respectively. For the sake of convenience, in this paper we shall deal with the continuum limit. However, all our results are applicable to the more realistic case in which detector outputs are treated as finite dimensional vectors. It is easy to see that the set of all detector outputs form a vector space satisfying the usual axioms of a vector space. The starting point of our discussion is the definition of the scalar product. Given any two functions $x(t)$ and $y(t)$, their scalar product $\langle x, y\rangle$ is defined as [22–25]

$$\langle x, y\rangle = 2\int_0^\infty \frac{df}{S_h(f)}[X(f)Y^*(f) + X^*(f)Y(f)], \qquad (2.1)$$

where $X(f) \equiv \int_{-\infty}^{\infty} dt x(t)\exp(-2\pi i f t)$ is the Fourier transform of the function $x(t)$ [and similarly, $Y(f)$] and $S_h(f)$ is the one-sided noise power-spectral density of the detector. The scalar product in Eq. (2.1) is motivated by the likelihood of a known signal buried in a Gaussian, stationary background [37].

Among all vectors, of particular interest are those corresponding to gravitational waves from a given astronomical source. While every signal can be thought of as a vector in the infinite-dimensional vector space of the detector outputs, the set of all such signal vectors do not, by themselves, form a vector space. One can immediately see that the norm of a signal h (i.e., the square root of the scalar product of a signal with itself) gives the SNR ρ using an optimal template [38,39]:

$$\rho \equiv \langle h, h\rangle^{1/2} = 2\left[\int_0^\infty \frac{df}{S_h(f)}|H(f)|^2\right]^{1/2}, \qquad (2.2)$$

where $H(f)$ is the Fourier transform of the signal $h(t)$. In particular, we can define signals $\hat{h}$ of unit norm:

$$\hat{h} \equiv \frac{h}{\sqrt{\langle h, h\rangle}} = \frac{h}{\rho}, \qquad \langle \hat{h}, \hat{h}\rangle = 1. \qquad (2.3)$$

The set of all normed signal vectors (i.e., signal vectors of unit norm) form a manifold, the parameters of the signal serving as a coordinate system [29,30,35,36]. Thus, each class of astronomical source forms an n-dimensional manifold $\mathcal{S}_n$, where n is the number of independent parameters characterizing the source. For instance, the set of all signals from a binary on a quasicircular orbit inclined to the line of sight at an angle ι, consisting of nonspinning black holes of masses m_1, and m_2, located a distance D from the Earth[1] initially in the direction (θ, φ) and expected to merge at a time t_C with the phase of the signal at merger φ_C, forms a nine-dimensional manifold with coordinates $\{D, \theta, \varphi, m_1, m_2, t_C, \varphi_C, \iota, \psi\}$, where ψ is the polarization angle of the signal. In the general case of a signal characterized by n parameters we shall denote the parameters by p^α, where $\alpha = 1, \ldots, n$. It should be noted that it is not possible in general to determine all the parameters of a signal using measurements from a single detector. In this case, we work with the submanifold with coordinates given by the determinable parameters.

The manifold $\mathcal{S}_n$ can be endowed with a metric $g_{\alpha\beta}$ that is induced by the scalar product defined in Eq. (2.1). The components of the metric in a coordinate system p^α are defined by[2]

$$g_{\alpha\beta} \equiv \langle \partial_\alpha \hat{h}, \partial_\beta \hat{h}\rangle, \qquad \partial_\alpha \hat{h} \equiv \frac{\partial \hat{h}}{\partial p^\alpha}. \qquad (2.4)$$

The metric can then be used on the signal manifold as a measure of the proper distance $d\ell$ between nearby signals with coordinates p^α and $p^\alpha + \mathrm{d}p^\alpha$, that is signals $\hat{h}(p^\alpha)$ and $\hat{h}(p^\alpha + \mathrm{d}p^\alpha)$,

$$d\ell^2 = g_{\alpha\beta} dp^\alpha dp^\beta. \qquad (2.5)$$

Now, by Taylor expanding $\hat{h}(p^\alpha + dp^\alpha)$ around p^α, and keeping only terms to second order in dp^α, it is straightforward to see that the overlap $\mathcal{O}$ of two infinitesimally close-by signals can be computed using the metric:

$$\begin{aligned}\mathcal{O}(dp^\alpha; p^\alpha) &\equiv \langle \hat{h}(p^\alpha), \hat{h}(p^\alpha + dp^\alpha)\rangle \\ &= 1 - \tfrac{1}{2} g_{\alpha\beta} dp^\alpha dp^\beta. \end{aligned} \qquad (2.6)$$

The metric on the signal manifold is nothing but the well-known Fisher information matrix usually denoted $\Gamma_{\alpha\beta}$ (see, e.g., [37,40]) but scaled down by the square of the SNR, i.e., $g_{\alpha\beta} = \rho^{-2}\Gamma_{\alpha\beta}$. The information matrix is itself the inverse of the covariance matrix $C_{\alpha\beta}$ and is a very useful quantity in signal analysis. The ambiguity function $\mathcal{A}(dp^\alpha; p^\alpha)$, familiar to signal analysts, is the overlap function defined above as $\mathcal{A}(dp^\alpha; p^\alpha) \simeq \mathcal{O}(dp^\alpha; p^\alpha)$. Thus, the equation

$$\mathcal{A}(dp^\alpha; p^\alpha) = \epsilon, \quad \text{or} \quad \mathcal{O}(dp^\alpha; p^\alpha) = \epsilon, \qquad (2.7)$$

where ϵ $(0 < \epsilon < 1)$ is a constant, defines the ambiguity

[1] Even though we deal with normed signals (which amounts to fixing D), astrophysical gravitational-wave signals are characterized by this additional parameter.

[2] We have followed the definition of the metric as is conventional in parameter estimation theory (see, e.g., Refs. [23–25,30]) which differs from that used in template placement algorithms (see, e.g., Refs. [35]) by a factor of 2. This difference will impact the relationship between the metric and the match as will be apparent in what follows.

surface, or level surface. In gravitational-wave literature ϵ, which measures the overlap between two mismatched signals, is also called the *match*. Using the expression for the overlap $\mathcal{O}$ [cf. Eq. (2.6)] in Eq. (2.7), we can see that the coordinate distance dp^α to the ambiguity surface from the coordinate point p^α is related to the proper distance[3] by

$$g_{\alpha\beta}dp^\alpha dp^\beta = 2(1-\epsilon). \tag{2.8}$$

Equivalently, $d\ell = \sqrt{2(1-\epsilon)}$. For a given value of the match ϵ the above equation defines a $(n-1)$-dimensional ellipsoid in the n-dimensional signal manifold. Every signal with parameters $p^\alpha + dp^\alpha$ on the ellipsoid has an overlap ϵ with the reference signal at p^α.

B. Coincidence windows

Having defined the metric (equivalently, the information matrix) and the ambiguity function, we next consider the application of the geometric formalism in the estimation of statistical errors involved in the measurement of the parameters and then discuss how that information may be used in coincidence analysis. We closely follow the notation of Finn and Chernoff [23–25] to introduce the basic ideas and apply their results in the choice of coincidence windows.

Let us suppose a signal of known shape with parameters p^α is buried in background noise that is Gaussian and stationary. Since the signal shape is known one can use matched filtering to dig the signal out of noise. The measured parameters $\bar{p}^\alpha$ will, in general, differ from the true parameters of the signal.[4] Geometrically speaking, the noise vector displaces the signal vector and the process of matched filtering projects the (noise + signal) vector back on to the signal manifold. Thus, any nonzero noise will make it impossible to measure the true parameters of the signal. The best one can hope for is a proper statistical estimation of the influence of noise.

The posterior probability density function $\mathcal{P}$ of the parameters $\bar{p}^\alpha$ is given by a multivariate Gaussian distribution[5]:

$$\mathcal{P}(\Delta p^\alpha)d^n\Delta p = \frac{d^n\Delta p}{(2\pi)^{n/2}\sqrt{C}}\exp\Big[-\frac{1}{2}C^{-1}_{\alpha\beta}\Delta p^\alpha\Delta p^\beta\Big], \tag{2.9}$$

where n is the number of parameters, $\Delta p^\alpha = p^\alpha - \bar{p}^\alpha$, and $C_{\alpha\beta}$ is the covariance matrix, C being its determinant. Noting that $C^{-1}_{\alpha\beta} = \rho^2 g_{\alpha\beta}$, we can rewrite the above distribution as

$$\mathcal{P}(\Delta p^\alpha)d^n\Delta p = \frac{\rho^n\sqrt{g}d^n\Delta p}{(2\pi)^{n/2}}\exp\Big[-\frac{\rho^2}{2}g_{\alpha\beta}\Delta p^\alpha\Delta p^\beta\Big], \tag{2.10}$$

where we have used the fact that $C = 1/(\rho^{2n}g)$, g being the determinant of the metric $g_{\alpha\beta}$. Note that if we define new parameters $p'^\alpha = \rho p^\alpha$, then we have exactly the *same* distribution function for all SNRs, except the deviations Δp^α are scaled by ρ.

Let us first specialize to one dimension to illustrate what region of the parameter space one should associate with a given trigger. In one dimension the distribution of the deviation from the mean of the measured value of the parameter p is given by

$$\begin{aligned}\mathcal{P}(\Delta p)d\Delta p &= \frac{d\Delta p}{\sqrt{2\pi}\sigma}\exp\Big(-\frac{\Delta p^2}{2\sigma^2}\Big)\\ &= \frac{\rho\sqrt{g_{pp}}d\Delta p}{\sqrt{2\pi}}\exp\Big(-\frac{\rho^2}{2}g_{pp}\Delta p^2\Big),\end{aligned} \tag{2.11}$$

where, analogous to the n-dimensional case, we have used $\sigma^2 = 1/(\rho^2 g_{pp})$. Now, at a given SNR, what is the volume V_P in the parameter space such that the probability of finding the measured parameters $\bar{p}$ inside this volume is P? This volume is defined by

$$P = \int_{\Delta p\in V_P}\mathcal{P}(\Delta p)d\Delta p. \tag{2.12}$$

Although V_P is not unique it is customary to choose it to be centered around $\Delta p = 0$:

$$\begin{aligned}P &= \int_{(\Delta p/\sigma)^2\le r^2(P)}\frac{d\Delta p}{\sqrt{2\pi}\sigma}\exp\Big(-\frac{\Delta p^2}{2\sigma^2}\Big)\\ &= \int_{\rho^2 g_{pp}\Delta p^2\le r^2(P)}\frac{\rho\sqrt{g_{pp}}d\Delta p}{\sqrt{2\pi}}\exp\Big(-\frac{\rho^2 g_{pp}\Delta p^2}{2}\Big),\end{aligned} \tag{2.13}$$

where given P the above equation can be used to solve for $r(P)$ and it determines the range of integration. For instance, the volumes V_P corresponding to $P \simeq 0.683, 0.954, 0.997, \ldots$, are the familiar intervals $[-\sigma, \sigma]$, $[-2\sigma, 2\sigma]$, $[-3\sigma, 3\sigma]$, …, and the corresponding values of r are 1, 2, 3. Since $\sigma = 1/\sqrt{\rho^2 g_{pp}}$ we see that in terms of g_{pp} the above intervals translate to

$$\begin{aligned}&\frac{1}{\rho}\Big[-\frac{1}{\sqrt{g_{pp}}},\frac{1}{\sqrt{g_{pp}}}\Big],\qquad \frac{1}{\rho}\Big[-\frac{2}{\sqrt{g_{pp}}},\frac{2}{\sqrt{g_{pp}}}\Big],\\ &\qquad\qquad \frac{1}{\rho}\Big[-\frac{3}{\sqrt{g_{pp}}},\frac{3}{\sqrt{g_{pp}}}\Big],\ldots.\end{aligned} \tag{2.14}$$

Thus, for a given probability P, the volume V_P shrinks as

[3]Here the proper distance refers to the distance between the signal $\hat{h}(p^\alpha)$ at the coordinate point p^α and a signal $\hat{h}(p^\alpha + \mathrm{d}p^\alpha)$ with coordinates $p^\alpha + dp^\alpha$ on the ambiguity surface.

[4]In what follows we shall use an overline to distinguish the measured parameters from true parameters p^α.

[5]A Bayesian interpretation of $\mathcal{P}(\Delta p^\alpha)$ is the probability of having the true signal parameters to lie somewhere inside the ellipsoidal volume centered at the maximum likelihood point $\bar{p}^\alpha$. In this case the overlap test for determining the coincidence test is motivated by a test of concordance that the true signal parameters p^α should lie in the overlap region.

$1/\rho$. The maximum distance $d_{\max}$ within which we can expect to find "triggers" at a given P depends inversely on the SNR ρ: $d\ell = \sqrt{g_{pp}\Delta p^2} = r/\rho$. Therefore, for $P \simeq 0.954$, $r = 2$ and at an SNR of 5 the maximum distance is 0.4, which corresponds to a match of $\epsilon = 1 - \frac{1}{2}d\ell^2 = 0.92$. In other words, in one dimension 95% of the time we expect our triggers to come from templates that have an overlap greater than or equal to 0.92 with the buried signal when the SNR is 5. This interpretation in terms of the match is a good approximation as long as $d\ell \ll 1$, which will be true for large SNR events. However, for weaker signals and/or greater values of P we cannot interpret the results in terms of the match although, the foregoing equation (2.12) can be used to determine $r(P)$. As an example, at $P \simeq 0.997$, $r = 3$ and at an SNR of $\rho = 4$ the maximum distance is $d\ell = 0.75$ and the match is $\epsilon = 23/32 \simeq 0.72$, which is significantly smaller than 1 and the quadratic approximation is not good enough to compute the match.

These results generalize to n dimensions. In n dimensions the volume V_P is defined by

$$P = \int_{\Delta p^\alpha \in V_P} \mathcal{P}(\Delta p^\alpha) d^n \Delta p. \tag{2.15}$$

Again, V_P is not unique but it is customary to center the volume around the point $\Delta p^\alpha = 0$:

$$P = \int_{\rho^2 g_{\alpha\beta}\Delta p^\alpha \Delta p^\beta \le r^2(P,n)} \frac{\rho^n \sqrt{g} d^n \Delta p}{(2\pi)^{n/2}} \times \exp\left[-\frac{\rho^2}{2} g_{\alpha\beta}\Delta p^\alpha \Delta p^\beta\right]. \tag{2.16}$$

Given P and the parameter space dimension n, one can iteratively solve the above equation for $r(P, n)$. The volume V_P is bounded by the surface defined by the equation

$$g_{\alpha\beta}\Delta p^\alpha \Delta p^\beta = \left(\frac{r}{\rho}\right)^2. \tag{2.17}$$

This is the same as the ellipsoid in Eq. (2.8) except that its size is defined by r/ρ. Let us note the generalization of a result discussed previously, namely that the size of the ellipsoid is not small enough for all combinations of P and ρ and, therefore, it is not always possible to interpret the distance from the center of the ellipsoid to its surface in terms of the overlap or match of the signals at the two locations except when the distance is close to zero. This is because the expression for the match in terms of the metric is based on the quadratic approximation which breaks down when the matches are small. However, the region defined by Eq. (2.17) always corresponds to the probability P and there is no approximation here (except that the detector noise is Gaussian).

When the SNR ρ is large and $1 - P$ is not close to zero, the triggers are found from the signal with matches greater than or equal to $1 - \frac{r^2(P,n)}{2\rho^2}$. Table I lists the value of r for several values of P in one, two, and three dimensions and the minimum match $\epsilon_{\rm MM}$ for SNRs of 5, 10, and 20. Table I should be interpreted in light of the fact that triggers come from an analysis pipeline in which the templates are laid out with a certain minimal match and one cannot, therefore, expect the triggers from different detectors to be matched better than the minimal match.

TABLE I. The value of the (squared) distance $d\ell^2 = r^2/\rho^2$ for several values of P and the corresponding smallest match that can be expected between templates and the signal at different values of the SNR.

	$P = 0.683$		$P = 0.954$		$P = 0.997$	
ρ	$d\ell^2$	$\epsilon_{\rm MM}$	$d\ell^2$	$\epsilon_{\rm MM}$	$d\ell^2$	$\epsilon_{\rm MM}$
			$n = 1$			
5	0.04	0.9899	0.16	0.9592	0.36	0.9055
10	0.01	0.9975	0.04	0.9899	0.09	0.9772
20	0.002 5	0.9994	0.01	0.9975	0.0225	0.9944
			$n = 2$			
5	0.092	0.9767	0.2470	0.9362	0.4800	0.8718
10	0.023	0.9942	0.0618	0.9844	0.1200	0.9695
20	0.005 75	0.9986	0.0154	0.9961	0.0300	0.9925
			$n = 3$			
5	0.141 2	0.9641	0.32	0.9165	0.568	0.8462
10	0.035 3	0.9911	0.08	0.9798	0.142	0.9638
20	0.008 83	0.9978	0.02	0.9950	0.0355	0.9911

From the table, we see that when the SNR is large (say greater than about 10) the dependence of the match $\epsilon_{\rm MM}$ on n is very weak; in other words, irrespective of the number of dimensions we expect the match between the trigger and the true signal (and for our purposes the match between triggers from different instruments) to be pretty close to 1, and mostly larger than a minimal match of about 0.95 that is typically used in a search. Even when the SNR is in the region of 5, for low P again there is a weak dependence of $\epsilon_{\rm MM}$ on the number of parameters. For large P and low SNR, however, the dependence of $\epsilon_{\rm MM}$ on the number of dimensions becomes important. At an SNR of 5 and $P \simeq 0.997$, $\epsilon_{\rm MM} = 0.91, 0.87, 0.85$, for $n = 1, 2, 3$ dimensions, respectively.

In general, for a given probability P the size of the ellipsoid at an SNR ρ is smaller by a factor ρ compared to that at $\rho = 1$. Thus, the volume in the parameter space in which the measured parameters will lie at a given probability P will scale with the SNR as ρ^{-n}. Therefore, if the goal of an experiment is to have false dismissal probability that is no greater than $1 - P$ then the ellipsoidal windows given by Eq. (2.17) could be employed when testing triggers from different detectors for coincidences. We now have our first result which states that:

When performing coincidence analysis of triggers one should test to see if the associated ellipsoids overlap with each other. These ellipsoids describe the smallest possible

volume within which the false dismissal probability is no more than a prespecified value.

Notice also that, if one assumes that false alarms are due to accidental coincidences between triggers which are otherwise uncorrelated,[6] the false alarm rate would then also go down by ρ^{-n}. Thus, given the false dismissal probability $1 - P$ the size of the ellipsoid further depends on the SNR of the events that are being subject to coincidence analysis, the size shrinking sharply as a function of the event's SNR. Thus we have the second of our results:

The size of the ellipsoids should be chosen in inverse proportion to the signal-to-noise ratio.

However, this latter feature has not yet been implemented in current gravitational-wave searches and will be a priority for implementation in future versions of the search pipeline [41]. The final, and practically speaking probably the most important result is the following:

Our coincidence algorithm reduces the number of tunable parameters from n (where n is the number of parameters) to 1, irrespective of the dimensionality of the signal parameter space.

The tunable parameter, μ, which will be introduced in Eq. (3.2), essentially scales the volume of the ambiguity ellipsoid. The appropriate value of this parameter can be determined by extensive Monte Carlo tests, for example by injecting fake signals into interferometer data, and optimizing the detection efficiency *vis-à-vis* false alarm rate. Having just one parameter greatly simplifies the tuning procedure.

III. OVERLAP OF ELLIPSOIDS

A key tool in determining coincidences of triggers from two or more detectors is a mathematical algorithm to determine if the ellipsoids associated with triggers either touch or overlap with each other. This algorithm forms the workhorse for identifying coincidence of triggers from two or more detectors.

As stated in Sec. II A, triggers resulting from the analysis pipeline are projections of the data by normed signal vectors onto an n-dimensional space $\mathcal{S}_n$, where n is the number of independent parameters characterizing the source. In the foregoing section we introduced ellipsoidal regions in the n-dimensional parameter space with their centers at the location of the maximum likelihood point. When we analyze the data, however, we will not know beforehand if a signal is present in the data and even when there is one we would not know where its location in the parameter space is. We will have, nevertheless, the knowledge of the location of the triggers in the parameter space. Let us denote the coordinates of a trigger from a detector A as q_A^α, where α is the index on the parameter space. The coincidence analysis proceeds in the following manner.

[6]This is not the case for colocated detectors such as the two LIGO Hanford interferometers.

Define an ellipsoidal region $\mathcal{E}(\mathbf{p}_A, \bar{g})$ around each trigger q_A^α by

$$\mathcal{E}(\mathbf{p}_A, \bar{g}) = \{\mathbf{p}_A \in \mathcal{S}_n | (\mathbf{p}_A - \mathbf{q}_A)^T \bar{g} (\mathbf{p}_A - \mathbf{q}_A) \leq 1\}, \tag{3.1}$$

where $\mathbf{q}_A \in \mathcal{S}_n$ is the position vector of the center of the ellipsoid (i.e., the location of the trigger from detector A) and $\bar{g}$ is the rescaled metric which we shall refer to as the *shape matrix*. It is related to the metric by

$$\bar{g}_{\alpha\beta} = \mu^2 g_{\alpha\beta}, \tag{3.2}$$

where μ^2 is a numerical scaling factor used to expand the linear distances of the ellipsoid while holding the position of the center and the spatial orientation constant. Equation (2.17) allows us to interpret the parameter μ in terms of the probability P with which the trigger can be expected to be found within the ellipsoid $\mathcal{E}(\mathbf{p}_A, \bar{g})$:

$$\mu^2 = \frac{\rho^2}{r^2(P)}. \tag{3.3}$$

Further, the probabilities P associated with a given μ can be found using Eq. (2.16) when the background noise is Gaussian. However, most detector noise is non-Gaussian and nonstationary and in those cases μ serves as a parameter that must be tuned to achieve a certain detection efficiency or, alternatively, a certain false alarm rate.

Note that the ellipsoids associated with high-SNR triggers are expected to overlap (and hence pass coincidence) even if they each have a smaller volume. On the other hand, for weaker signals we need to associate larger ellipsoids in order for them to overlap.

Thus, the shape matrix is the scaled metric and encodes the local correlations between the parameters in the neighborhood of the trigger. It is trivial to check that when $\mu = 1$, Eq. (3.1) defines the interior of the ambiguity ellipsoid previously defined in Eq. (2.7).

Once an ellipsoidal model for the trigger is established, following [42] one can construct a contact function $\mathcal{F}_{AB}(\lambda)$ of two ellipsoids $\mathcal{E}(\mathbf{q}_A, \bar{g}_A)$ and $\mathcal{E}(\mathbf{q}_B, \bar{g}_B)$ (defined around triggers from detectors A and B) as

$$\mathcal{F}_{AB}(\lambda) = \lambda(1-\lambda)\mathbf{r}_{AB}^T [\lambda \bar{g}_B^{-1} + (1-\lambda)\bar{g}_A^{-1}]^{-1} \mathbf{r}_{AB}, \tag{3.4}$$

where $\mathbf{r}_{AB} = \mathbf{q}_B - \mathbf{q}_A$ and $\lambda \in [0, 1]$ is a scalar parameter. The maximum of the contact function over λ in the interval [0, 1] can be shown [42] to be unique. It can also be shown that for two overlapping ellipsoids, the maximum of the contact function is less than 1, i.e.,

$$F = \max_{0 \leq \lambda \leq 1} [\mathcal{F}_{AB}(\lambda)] < 1. \tag{3.5}$$

When $F = 1$, the two ellipsoids "touch" each other ex-

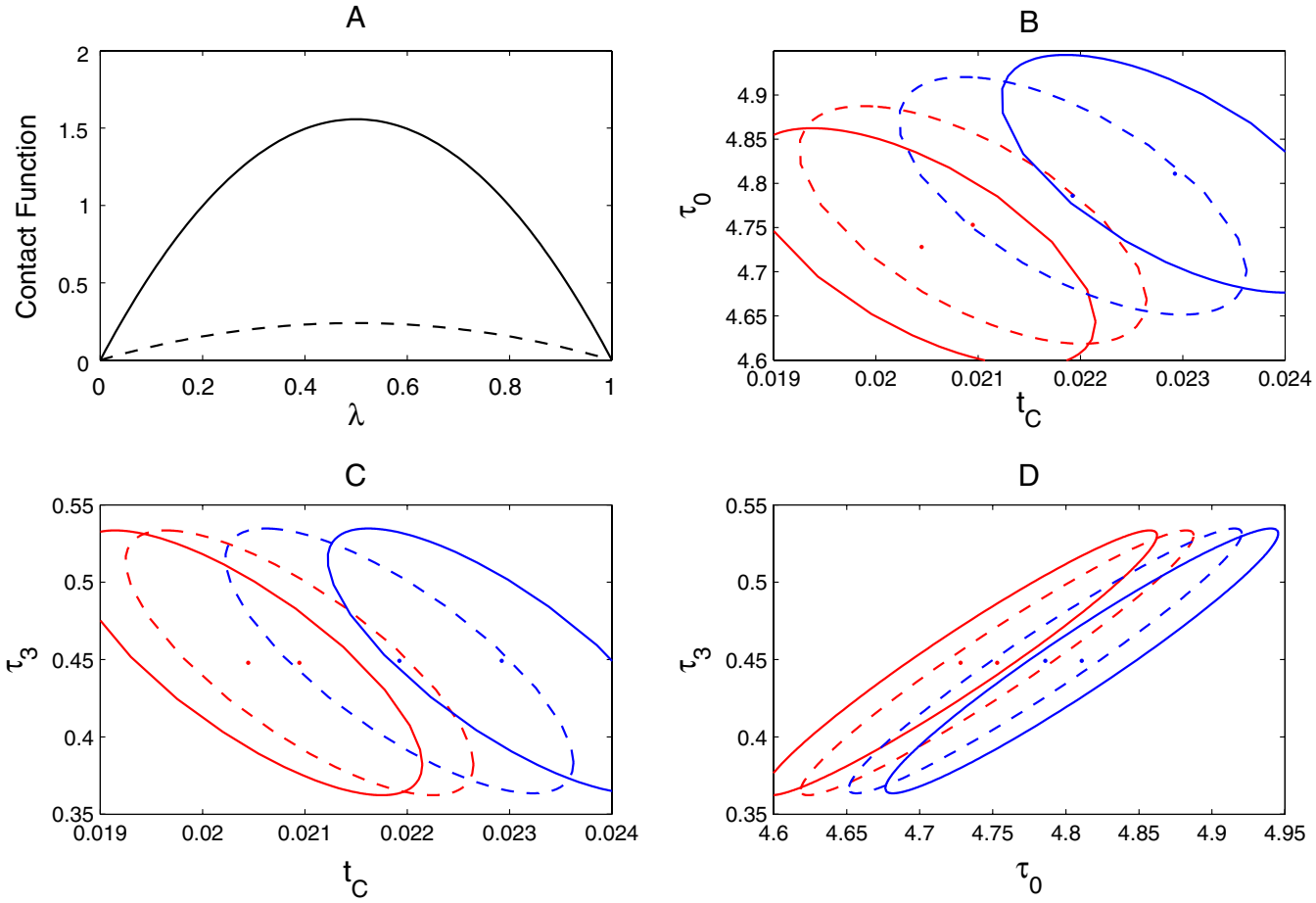

FIG. 1 (color online). (a) plots the contact function Eq. (3.4) for two pairs of three-dimensional ellipsoids taken from a search for binaries consisting of nonspinning compact objects characterized by parameters (t_c, τ_0, τ_3) [see Sec. V, in particular, Eq. (5.4)]. (b)–(d) are the projections of the ellipsoids in (t_c, τ_0), (t_c, τ_3), and (τ_0, τ_3) orthogonal planes, respectively. Solid lines refer to the case of nonoverlapping ellipsoids and dashed lines are for overlapping (i.e., coincident) triggers. Note that in the latter case the maximum of the contact function is ≤ 1, which is the test that is carried out to determine if a pair of triggers are in coincidence.

ternally. Figure 1 shows the contact function in the case of overlapping and nonoverlapping ellipsoids.

In the ''coincidence'' data-analysis paradigm, given triggers from N detectors ($N \geq 2$), one draws up a list of ''coincident triggers'' for further analysis to test their significance. The simplest coincident triggers consist of those which have ''consistent'' parameters in two detectors (two-way coincidence). Testing for two-way coincidences for triggers from colocated detectors (e.g., the two LIGO detectors at Hanford) can be accomplished by a single test of Eq. (3.5) on a pair of triggers.

When the detectors are noncolocated, one needs to allow for a nonzero ''time-of-flight'' delay between the trigger arrival times. One assumes that the GW signals travel at the speed of electromagnetic radiation in vacuum c and the maximum allowed time delay is then set to $\pm\Delta/c$, where Δ is the distance between the two detectors. As far as the geometrical picture of the coincidence test is concerned, for the noncolocated case one needs to test for the overlap of a ''cylindrical'' volume (of length $2\Delta/c$ along the time dimension) and an ellipsoid.[7] In practice, however, the test can be carried out iteratively by adding discrete time delays to the trigger (spanning the allowed time delay) from one detector and testing for the overlap condition against the trigger from the other detector, keeping the latter fixed in time. The discrete time step can be set to the inverse of the sampling frequency of the time series. The fact that the overlap test is computationally cheap allows for such a brute-force implementation strategy to be viable.

These 2-way coincident triggers can now be used as building blocks to construct more complex coincidence triggers that have consistent parameters over three or more interferometers (3-way, . . ., n-way coincidence triggers). For example, the set of triggers (T_A, T_B, T_C) can be

[7]Note that, in the case of an externally triggered search, where the position of the source is known, we can use a fixed time delay for noncolocated detectors.

classified as 3-way coincident if (T_A, T_B), (T_B, T_C), and (T_A, T_C) 2-way coincident pairs exist. Here again, the subscripts $A \neq B \neq C$ are labels on interferometers. This idea can be generalized to determine the list of n-way coincident triggers given the list of $(n-1)$-way coincidences. It is useful to note that Eq. (3.5) is the only test we need in order to build the entire hierarchy of coincidence triggers.

We conclude this section by drawing attention to two practical issues in implementing this geometrical coincidence test. The first has to do with the algorithm one uses to draw up two-way coincidences. Given the set of triggers from two detectors, one can (a) work with time-ordered triggers and (b) find the maximum length of the bounding box of the ellipsoid along the time dimension over all the triggers such that for any trigger from one detector, the test for overlap is carried out only if a trigger from the other detector occurs at a time that is within twice this interval. This approach greatly reduces the overall number of overlap tests required to find two-way coincidences. The expression for the length of the sides of the bounding box can be algebraically determined given the shape matrix of the triggers and is explicitly given for 2 and 3 dimensions in the next section.

The second point is about the numerical implementation of the test of the overlap of ellipsoids where we maximize the contact function over a single parameter λ. Evaluation of the contact function involves matrix inversion which can be computationally quite expensive. Under these circumstances, prior knowledge of the inverse of trigger shape matrices can prove to be more efficient than on-the-fly computation. Brent's minimization method [43,44] is particularly suitable for fast convergence to the maxima given the well-behaved nature of the contact function and is available as part of the GNU Scientific Library [45].

IV. EXPECTED REDUCTION IN FALSE ALARM RATE

Next, let us consider the reduction in the false alarm rate as a result of using ellipsoidal windows as opposed to rectangular windows.[8] In order to achieve false dismissal probability less than or equal to $1-P$, a rectangular window has to be at least as large as the box that encloses the ellipsoid. Now the volume of an n-dimensional ellipsoid ($n \geq 2$) whose semiaxes are a_k, $k = 1, \ldots, n$, is given by a recursive formula:

$$V_n = \frac{2\pi V_{n-2}}{n} \prod_{k=1}^{n} a_k, \quad \text{where } V_0 = 1, \qquad V_1 = 2. \tag{4.1}$$

On the other hand, the smallest volume an n-dimensional box that encloses the ellipsoid would be

$$U_n = \prod_{k=1}^{n} (2a_k) = 2^n \prod_{k=1}^{n} a_k, \tag{4.2}$$

where a factor of 2 arises since a_k are semimajor axes and the side lengths of the enclosing box will be twice that value. Thus, the rectangular box's volume is larger than that of the ellipsoid by the factor

$$r \equiv \frac{U_n}{V_n} = \frac{n 2^{n-1}}{\pi V_{n-2}}. \tag{4.3}$$

Thus, in 2, 3, and 4 dimensions the savings are $4/\pi$, $6/\pi$, and $32/\pi^2$, respectively. However, the real factor could be far greater as the error ellipsoids are generally not oriented along the coordinate axes.

When the ellipsoid is not aligned with the coordinate axes, which will be the case when there are correlations between the different parameters, the side lengths of the bounding box are given by maximizing each coordinate axis over the entire ellipsoidal surface as follows. Starting from Eq. (2.17) one can express the first of the coordinates $p \equiv p^1$ in terms of the other coordinates:

$$\begin{aligned} &g_{11}p^2 + 2g_{1i}pp^i + g_{ij}p^i p^j - \left(\frac{r}{\rho}\right)^2 = 0, \\ &i, j = 2, \ldots, n, \end{aligned} \tag{4.4}$$

which can be solved to obtain

$$p_{\pm} = \frac{1}{g_{11}}[-g_{1i}p^i \pm \sqrt{(g_{1i}g_{1j} - g_{11}g_{ij})p^i p^j + (g_{11}r^2/\rho^2)}]. \tag{4.5}$$

For our purposes we only need the "plus" solution. One can then set up $n-1$ equations in as many variables by demanding that $\partial p_+ / \partial p^k = 0$, which gives

$$\left[\frac{(g_{1i}g_{1k} - g_{11}g_{ik})(g_{1j}g_{1k} - g_{11}g_{jk})}{g_{1k}^2} - (g_{1i}g_{1j} - g_{11}g_{ij})\right] \times p^i p^j = g_{11}\frac{r^2}{\rho^2}. \tag{4.6}$$

These are again quadratic equations that must be solved (simultaneously) for the coordinates p^j, $j = 2, \ldots, n$. The resulting (positive) roots, denoted p_1^j can be substituted in Eq. (4.4) to obtain the half side length of the ellipse. We shall next give explicit expressions for the side lengths of the enclosing box in two and three dimensions. In higher dimensions the expressions are rather cumbersome but the general procedure outlined above can be used to compute the volume of the bounding box in all cases.

The side lengths of the bounding box are given in two dimensions by

[8] This discussion again assumes that false alarms are due to accidental coincidences between otherwise uncorrelated triggers.

$$x = 2\sqrt{\frac{\bar{g}_{22}}{|\bar{g}|}}, \qquad y = 2\sqrt{\frac{\bar{g}_{11}}{|\bar{g}|}}, \tag{4.7}$$

and in three dimensions by

$$x = 2\sqrt{\frac{(\bar{g}_{23}^2 - \bar{g}_{22}\bar{g}_{33})\bar{g}_{22}}{(\bar{g}_{12}\bar{g}_{23} - \bar{g}_{22}\bar{g}_{13})^2 - (\bar{g}_{23}^2 - \bar{g}_{22}\bar{g}_{33})(\bar{g}_{12}^2 - \bar{g}_{11}\bar{g}_{22})}},$$
$$y = 2\sqrt{\frac{(\bar{g}_{13}^2 - \bar{g}_{11}\bar{g}_{33})\bar{g}_{11}}{(\bar{g}_{12}\bar{g}_{13} - \bar{g}_{11}\bar{g}_{23})^2 - (\bar{g}_{13}^2 - \bar{g}_{11}\bar{g}_{33})(\bar{g}_{12}^2 - \bar{g}_{11}\bar{g}_{22})}},$$
$$z = 2\sqrt{\frac{(\bar{g}_{12}^2 - \bar{g}_{11}\bar{g}_{22})\bar{g}_{11}}{(\bar{g}_{12}\bar{g}_{13} - \bar{g}_{11}\bar{g}_{23})^2 - (\bar{g}_{12}^2 - \bar{g}_{11}\bar{g}_{22})(\bar{g}_{13}^2 - \bar{g}_{11}\bar{g}_{33})}}. \tag{4.8}$$

V. APPLICATION TO COALESCING BINARIES

Inspiralling compact binaries are one of the most promising candidates for detection by the laser interferometric detectors. It will, therefore, be interesting to investigate the gains of using the new coincidence method in such searches. For the purpose of our discussion, it will suffice to use a simple model of the signal. We shall use the Fourier representation of the waveform from a binary consisting of nonspinning compact objects on a quasicircular orbit in which post-Newtonian corrections to the amplitude are neglected, but corrections to the phase are included to the desired order. This waveform is calculated using the stationary phase approximation, and is of the form:

$$\tilde{h}(f) = \frac{AM^{5/6}}{D\pi^{2/3}}\sqrt{\frac{5\eta}{24}} f^{-7/6} \exp\left[i\Psi(f; t_C, \phi_C, k) + i\frac{\pi}{4}\right], \tag{5.1}$$

$$\Psi(f) = 2\pi f t_C + \phi_C + \sum_k \lambda_k f^{(k-5)/3}, \tag{5.2}$$

where M is the total mass of the system, and η is the symmetric mass ratio, which is defined as $\eta \equiv m_1 m_2/M^2$. D is the distance to the source, and A is a constant which depends on the relative orientations of the detector and the binary orbit, and t_C and ϕ_C are as defined in Sec. II A. Waveforms of this type at second post-Newtonian order [46,47] have been used in previous searches for binary neutron star inspirals [12], and are currently being used in searches for compact binary inspirals with a total mass of $<35M_\odot$ [41]. Moreover, the metric computed for such a waveform has been shown to be approximately valid for a range of physical approximants [48,49]. At the 2PN order, the coefficients λ_k are given by the following expressions:

$$\lambda_0 = \frac{3}{128\eta(\pi M)^{5/3}}, \qquad \lambda_1 = 0,$$
$$\lambda_2 = \frac{5}{96\pi\eta M}\left(\frac{743}{336} + \frac{11}{4}\eta\right), \qquad \lambda_3 = \frac{-3\pi^{1/3}}{8\eta M^{2/3}}, \tag{5.3}$$
$$\lambda_4 = \frac{15}{64\eta(\pi M^{1/3}}\left(\frac{3058673}{1016064} + \frac{5429}{1008}\eta + \frac{617}{144}\eta^2\right).$$

The metric required for determining coincidence in the case of nonspinning binaries is that in the three-dimensional space of (t_C, τ_0, τ_3), where τ_0 and τ_3 are the chirp times, which are a convenient way of parametrizing the masses of the binary system. They are given by

$$\tau_0 = \frac{5}{256\pi f_L \eta}(\pi M f_L)^{-5/3},$$
$$\tau_3 = \frac{1}{8 f_L \eta}(\pi M f_L)^{-2/3}, \tag{5.4}$$

where f_L is the frequency below which no appreciable signal can be detected due to rising detector noise at low frequencies.

In obtaining the metric, it proves to be more convenient to use parameters $(t_C, \theta_1, \theta_2)$, where $\theta_1 \equiv 2\pi f_L \tau_0$, and $\theta_2 \equiv 2\pi f_L \tau_3$. This metric was obtained by Owen in [35]. Here, Eq. (2.6) was used, and the phase ϕ_C maximized over to give the expression for the metric:

$$g_{\alpha\beta} = \tfrac{1}{2}(\mathcal{J}[\psi_\alpha\psi_\beta] - \mathcal{J}[\psi_\alpha]\mathcal{J}[\psi_\beta]), \tag{5.5}$$

where ψ_α is the derivative of the Fourier phase of the inspiral waveform with respect to parameter θ_α. $\mathcal{J}$ is the moment functional of the noise power spectral density (PSD), which is defined for any function $a(x)$ as

$$\mathcal{J}(a) \equiv \frac{1}{I(7)}\int_{x_L}^{x_U} \frac{a(x)x^{-7/3}}{S_h(x)}dx. \tag{5.6}$$

$I(q)$ is the qth moment of the noise PSD, which is defined by

$$I(q) \equiv S_h(f_0)\int_{x_L}^{x_U} \frac{x^{-q/3}}{S_h(x)}dx, \tag{5.7}$$

where $x \equiv f/f_0$, with f_0 being a fiducial frequency used to set the range of the numerical values of the functions contained in the integrals. The value of x_L is chosen so that the contribution to the integral for values below x_L would be negligible. $x_U \equiv f_U/f_0$, where f_U is the ending frequency of the inspiral waveform in question. In deriving the explicit expression for the metric, the starting point is the Fourier phase of the waveform in the form [48]:

$$\Psi(f; t_C, \theta_1, \theta_2) = 2\pi f t_C + a_{01}\theta_1 x^{-5/3} + [a_{21}(\theta_1/\theta_2) + a_{22}(\theta_1\theta_2^2)^{1/3}]x^{-1} + a_{31}\theta_2 x^{-2/3} + [a_{41}(\theta_1/\theta_2^2) + a_{42}(\theta_1/\theta_2)^{1/3} + a_{43}(\theta_2^4/\theta_1)^{1/3}]x^{-1/3}, \tag{5.8}$$

where the coefficients a_{km} are given by

$$a_{01} = \frac{3}{5}, \quad a_{21} = \frac{11\pi}{12}, \quad a_{22} = \frac{743}{2016}\left(\frac{25}{2\pi^2}\right)^{1/3},$$
$$a_{31} = \frac{-3}{2}, \quad a_{41} = \frac{617}{384}\pi^2, \quad a_{42} = \frac{5429}{5376}\left(\frac{25\pi}{2}\right)^{1/3},$$
$$a_{43} = \frac{15\,293\,365}{10\,838\,016}\left(\frac{5}{4\pi^4}\right)^{1/3}. \tag{5.9}$$

Using the above in Eq. (5.5), one can find an explicit expression for the metric. The expression can be obtained [48] by utilizing the fact that, since the Fourier phase is a polynomial function, $\mathcal{J}$ can be expanded in terms of normalized moments J, where

$$J(p) \equiv \frac{I(p)}{I(7)}. \tag{5.10}$$

To assess the potential gains of using this coincidence method for inspiral analysis, it is useful to consider the difference in volume between the ellipsoidal region defined by $\bar{g}$, and its bounding box aligned with the coordinate axes (t_C, τ_0, τ_3). This ratio can be calculated with the help of Eqs. (4.8). Figure 2 shows how this ratio varies across the (τ_0, τ_3) space in the case of Initial and Advanced LIGO, Virgo and Einstein Telescope (a third generation European detector that is currently being designed). It can be seen that for most of the parameter space, the volume of the bounding box is an order of magnitude larger than the volume of the ellipsoid; however, in certain regions, corresponding to high masses, this ratio can be as large as 2 orders of magnitude. This suggests that significant reductions of the background can be achieved by using ellipsoidal windows. Runs on example data sets suggest that in practice, the reduction in background coincident triggers due to using such a coincidence method will be a factor of $\sim$10.

To assess the improvement in the confidence in any candidate detection, it is helpful to look at how reducing

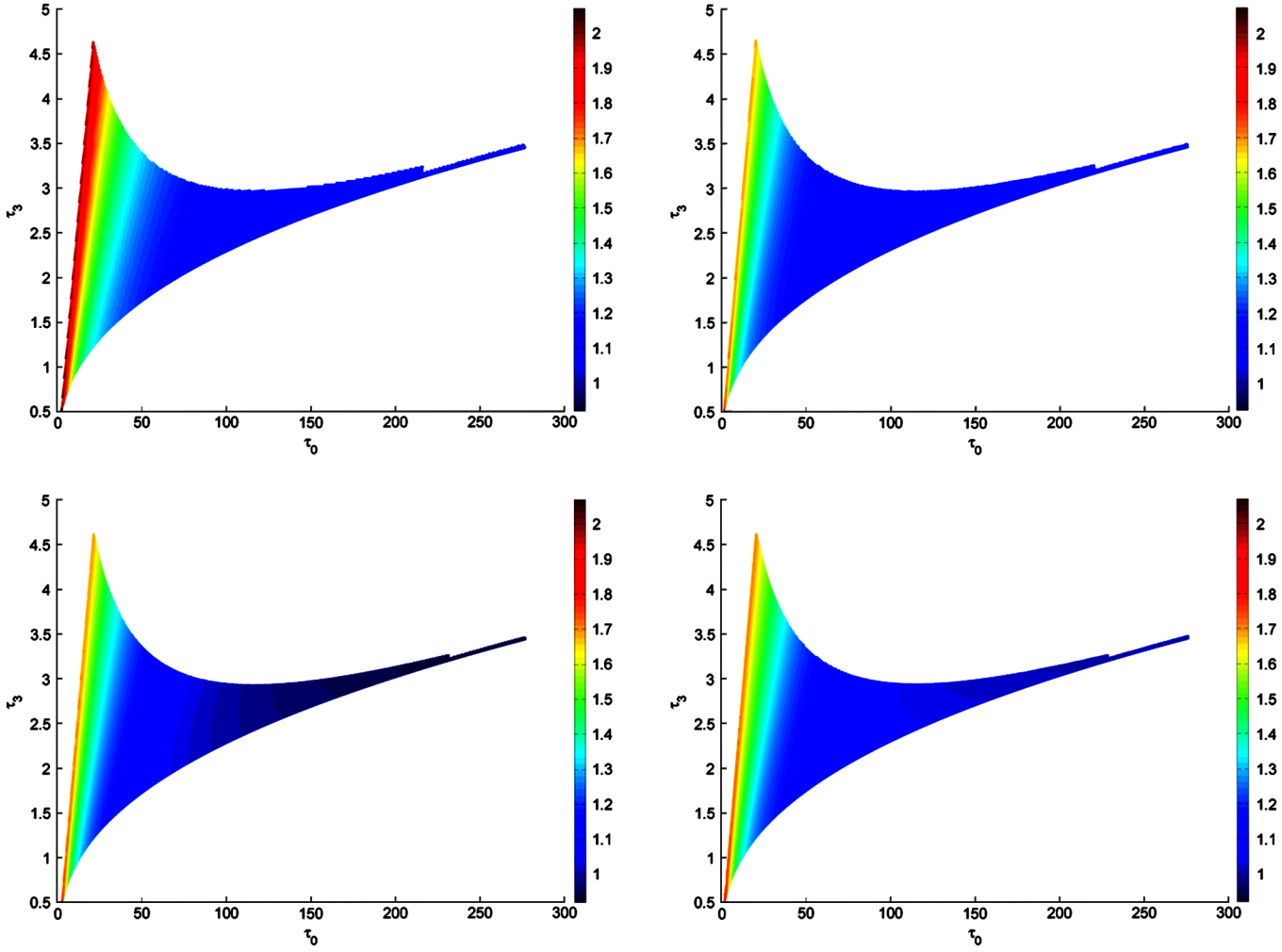

FIG. 2 (color online). The $\log_{10}$ of the ratio of the volume of the bounding box to the volume of the ellipsoid as a function of location in (τ_0, τ_3) space. The plots shown are (clockwise from top right) for the initial LIGO, advanced LIGO, Virgo, and Einstein Telescope. The low frequency cutoff is chosen to be 20 Hz.

the background rate by a factor of k will improve the odds O of a detection

$$O(h \mid D) = \frac{P(h \mid D)}{P(0 \mid D)}, \tag{5.11}$$

where $P(h \mid D)$ is the posterior probability of a signal h being present if the set of triggers D has been obtained, and $P(0 \mid D)$ is the probability of there being no signal given D. We take the accidental trigger rate to be a Poisson process, with a trigger rate prior to reduction λ. Assuming that the detection efficiency is not affected by the reduction in the trigger rate, we see that the odds improve by the following factor:

$$\frac{O(h \mid D)_{\lambda/k}}{O(h \mid D)_{\lambda}} = \frac{1 - e^{-\lambda T}}{1 - e^{-\lambda T/k}}, \tag{5.12}$$

where T is the duration of the run.

After reducing the false alarm rate by a factor k, the odds of a signal being present improve by a factor which depends on how high the false alarm rate was to start with. If the initial false alarm rate is low ($\lambda T \ll 1$), the improvement in the odds approaches the factor k. However, for high false alarm rates, the improvement becomes less marked, tending to a factor of 1 as $\lambda T \to \infty$.

VI. SUMMARY AND CONCLUSIONS

A new method of coincidence analysis is proposed in which, instead of the rectangular windows on parameters conventionally used, ellipsoidal windows are employed based on the metric defined on the signal manifold. This allows us to use windows of appropriate size depending on the location in the parameter space, instead of using a phenomenological "best fit" choice of windows across the entire space. The algorithm has a massive practical advantage in that it requires the tuning of only one parameter irrespective of the number of dimensions of the parameters. This contrasts with the conventional method that required us to tune nearly as many parameters as the dimension of the parameter space. In addition, the method allows us to take into account covariances between parameters, thus significantly reducing the volume enclosed within the windows. In particular, for the case of nonspinning compact binary coalescence in Initial LIGO, it is expected that the use of such a method will reduce the background rate of coincident triggers by roughly an order of magnitude. By also incorporating SNR dependence into the size of the windows, the background of high-SNR events can be reduced even further.

The algorithm has been implemented in C code in the LSC Algorithm Library (LAL) [50]. An implementation in (t_C, τ_0, τ_3) space, as in Sec. V, using SNR-independent windows, is being employed in the search for compact binary coalescence in S5 data. This implementation is referred to as *e-thinca* [41].

ACKNOWLEDGMENTS

The authors gratefully acknowledge the members of the Compact Binary Coalescence working group of the LIGO Scientific Collaboration for their contributions, suggestions, and discussions regarding this work. The authors are also grateful to Alan Weinstein, Michele Valisneri, Alexander Dietz, and Duncan Brown for carefully reading the manuscript and for suggesting improvements to the text.

[1] B. Abbott *et al.* (LIGO Scientific Collaboration), Nucl. Instrum. Methods Phys. Res., Sect. A **517**, 154 (2004).
[2] F. Acernese *et al.*, Classical Quantum Gravity **23**, S635 (2006).
[3] H. Luck *et al.*, Classical Quantum Gravity **23**, S71 (2006).
[4] A. Pai, S. Dhurandhar, and S. Bose, Phys. Rev. D **64**, 042004 (2001).
[5] S. Bose, S. V. Dhurandhar, and A. Pai, Pramana **53**, 1125 (1999).
[6] L. S. Finn, Phys. Rev. D **63**, 102001 (2001).
[7] N. Arnaud *et al.*, Phys. Rev. D **68**, 102001 (2003).
[8] P. Jaranowski and A. Krolak, Phys. Rev. D **49**, 1723 (1994).
[9] P. Jaranowski and A. Krolak, Classical Quantum Gravity **13**, 1279 (1996).
[10] H. Tagoshi *et al.*, Phys. Rev. D **75**, 087306 (2007).
[11] B. Abbott *et al.* (LIGO Scientific Collaboration), Phys. Rev. D **69**, 122001 (2004).
[12] B. Abbott *et al.* (LIGO Scientific Collaboration), Phys. Rev. D **72**, 082001 (2005).
[13] B. Abbott *et al.* (LIGO Scientific Collaboration), Phys. Rev. D **72**, 082002 (2005).
[14] B. Abbott *et al.* (LIGO Scientific Collaboration), Phys. Rev. D **73**, 062001 (2006).
[15] N. Arnaud *et al.*, Phys. Rev. D **65**, 042004 (2002).
[16] H. Mukhopadhyay, N. Sago, H. Tagoshi, S. Dhurandhar, H. Takahashi, and N. Kanda, Phys. Rev. D **74**, 083005 (2006).
[17] B. Abbott *et al.* (LIGO Scientific Collaboration), Phys. Rev. D **72**, 062001 (2005).
[18] B. Abbott *et al.* (LIGO Scientific Collaboration), Classical Quantum Gravity **23**, S29 (2006).
[19] H. Takahashi *et al.* (TAMA Collaboration and LISM Collaboration), Phys. Rev. D **70**, 042003 (2004).
[20] B. Abbott *et al.* (LIGO Collaboration), Phys. Rev. D **73**, 102002 (2006).
[21] K. Cannon, arXiv:g070881-00-Z.

[22] C. Cutler and E. Flanagan, Phys. Rev. D **49**, 2658 (1994).
[23] L. Finn, Phys. Rev. D **46**, 5236 (1992).
[24] L. Finn and D. Chernoff, Phys. Rev. D **47**, 2198 (1993).
[25] D. F. Chernoff and L. S. Finn, Astrophys. J. **411**, L5 (1993).
[26] K. Kokkotas, A. Królak, and G. Tsegas, Classical Quantum Gravity **11**, 1901 (1994).
[27] A. Królak, K. Kokkotas, and G. Schäfer, Phys. Rev. D **52**, 2089 (1995).
[28] E. Poisson and C. Will, Phys. Rev. D **52**, 848 (1995).
[29] R. Balasubramanian, B. S. Sathyaprakash, and S. V. Dhurandhar, Pramana **45**, L463 (1995).
[30] R. Balasubramanian, B. S. Sathyaprakash, and S. V. Dhurandhar, Phys. Rev. D **53**, 3033 (1996); **54**, 1860(E) (1996).
[31] E. E. Flanagan and S. A. Hughes, Phys. Rev. D **57**, 4566 (1998).
[32] K. G. Arun, B. R. Iyer, B. S. Sathyaprakash, and P. A. Sundararajan, Phys. Rev. D **71**, 084008 (2005); **72**, 069903(E) (2005).
[33] S.-i. Amari and H. Nagaoka, *Methods of Information Geometry* (American Mathematical Society, Providence, RI, 2000).
[34] B. S. Sathyaprakash, Phys. Rev. D **50**, R7111 (1994).
[35] B. Owen, Phys. Rev. D **53**, 6749 (1996).
[36] B. Owen and B. S. Sathyaprakash, Phys. Rev. D **60**, 022002 (1999).
[37] C. Helström, *Statistical Theory of Signal Detection*, International Series of Monographs in Electronics and Instrumentation Vol. 9 (Pergamon Press, Oxford, U.K., 1968), 2nd ed.
[38] K. S. Thorne, in *Three Hundred Years of Gravitation*, edited by S. Hawking and W. Israel (Cambridge University Press, Cambridge, England, 1987), pp. 330–458.
[39] B. Schutz, in *The Detection of Gravitational Waves*, edited by D. Blair (Cambridge University Press, Cambridge, England, 1989).
[40] Y. Pan, A. Buonanno, Y. Chen, and M. Vallisneri, Phys. Rev. D **69**, 104017 (2004).
[41] L. S. C. Compact Binary Coalescence Group (private communication).
[42] J. Perram and M. Wertheim, J. Comput. Phys. **58**, 409 (1985).
[43] Wikipedia Article, Brent's Method, http://en.wikipedia.org/wiki/Brent's_method.
[44] R. Brent, *Algorithms for Minimization Without Derivatives* (Prentice-Hall, Englewood Cliffs, NJ, 1973), Chap. 4.
[45] GSL, http://www.gnu.org/software/gsl/ (The GNU Scientific Library is a free numerical library licensed under the GNU GPL).
[46] L. Blanchet, T. Damour, and B. R. Iyer, Phys. Rev. D **51**, 5360 (1995).
[47] L. Blanchet, T. Damour, B. R. Iyer, C. M. Will, and A. G. Wiseman, Phys. Rev. Lett. **74**, 3515 (1995).
[48] S. Babak, R. Balasubramanian, D. Churches, T. Cokelaer, and B. Sathyaprakash, Classical Quantum Gravity **23**, 5477 (2006).
[49] T. Cokelaer, Phys. Rev. D **76**, 102004 (2007).
[50] LSC Algorithm Library, http://www.lsc-group.phys.uwm.edu/daswg/projects/lal.html.